Report on the 12-Inch Cyclotron Magnet Study: Measurements, Modeling, and Future plans.

Timothy W. Koeth
Rutgers University, Piscataway NJ 08854

ABSTRACT: A small 12-Inch, 1.2MeV proton cyclotron has been constructed for and is in instructional use in an upper level Physics lab course.[1] Every spring semester two exceptional students from the Modern Physics Lab class undertake an R&D project geared to improve the cyclotron's operation. This R&D project also affords the students a unique research experience. This document outlines the cumulative work of the author, several cyclotron staff members, and several students' efforts to measure, characterize, and upgrade the cyclotron's magnetic field in an attempt to improve the beam intensity.

I. MOTIVATION. Initially, to satisfy the cyclotron resonance condition, the pole tips of the 12-Inch Cyclotron magnet were Blanchard ground to provide parallelism to better than 1 part in 10,000. As will be seen, this pure vertical field does not provide any beam focusing effects, all but a very few of the generated ions are lost on either the top of bottom plate of the DEE. Indeed, during commissioning of the cyclotron, only a trickle of beam current, less than a nano-ampere, made it to the periphery. Desiring beam currents of at least 10μA in intensity, a program to study and modify the cyclotron to achieve this goal is under way.

Chun and McLynne[2] started this project by understanding and reporting the effects of the pole tip's boundary conditions and the resulting field. After much debate, a simple linear tapered pole tip design with an overall 2% decrease of B_z was settled upon. The magnet gap was to increase radially, starting from a minimum of 2.010 inches at r = 0 to 2.018 at r = 5.0 inches, the maximum possible ion radius. The author obtained the needed soft 1006 iron material. The pole tips were machined with azimuthal symmetry about r = 0.

Using a specially made measuring fixture McClain and Friedman characterized the vertical B-field, B_z, as a function of radius in the median plane. This characterization was along a single radial path, as opposed to a full 2D map. The assumption was initially held that the field was azimuthally uniform. That is, the contours of the field should form nice circles about r = 0.

II. FOCUSING THEORY. A quick review of orbit theory in a magnetic field which decreases with growing radius. This is colloquially known as weak focusing.

First we define the field index:

$$n = -\frac{r}{B}\frac{dB}{dr}$$

There are three possible cases:

1. $n < 0$ the field increases with r
2. $n = 0$ the field is uniform
3. $n > 0$ the field decreases with r

Axial Stability: Expand B_r by a Taylor expansion:

$$B_r = z\frac{\partial B_r}{\partial z}\bigg|_{z=0} + \frac{z^2}{2}\frac{\partial^2 B_r}{\partial z^2}\bigg|_{z=0} + \ldots$$

We consider only the first term of this expansion. From Maxwell's equations, we know:

$$\vec{\nabla} \times \vec{B} = 0$$

In considering azimuthal symmetry, we can say:

$$\frac{\partial B_r}{\partial z}\bigg|_{z=0} = \frac{\partial B_z}{\partial r}\bigg|_{z=0}$$

thus

$$B_r = z\frac{\partial B_r}{\partial z}\bigg|_{z=0} = z\frac{\partial B_z}{\partial r} = \frac{\partial B}{\partial r}z$$

Because $\frac{\partial B}{\partial r}z\big|_{z=0}$ has no radial component we can say $B_z = B$. From the above definition of the field index we write:

$$B_r = \frac{\partial B}{\partial r} = -nB\frac{z}{r}$$

Any field change in one axis corresponds to a change in the other. Thus if we can measure the change in the vertical component of the B-field we can make an inference of the change in the horizontal component.

Now, let us write the equations of motion for a particle of mass *m* in the magnetic field. First consider the restoring force that the particle will experience when taking an excursion from the median plane. We assume the force is proportional to the displacement:

$$F = m\ddot{z} = Kz$$

Then next consider the guiding field:

$$F_z = -qv_\theta B_r$$

where

$$v_\theta = \omega\theta$$

Substitute for B_r and equate to get

$$m\frac{d^2z}{dt^2} = -qvnB\frac{z}{r}$$

Re-arrange and again use $v_\theta = \omega\theta$ along with the cyclotron equation $m = \frac{qB}{\omega}$, and we get the well known Kerst-Serber Equation:

$$\frac{d^2z}{d^2t} + n\omega^2 z = 0$$

A solution of z = 0 is the unperturbed orbit, but another, and more interesting, solution is:

$$z = z_{\max}\sin\left(\sqrt{n}\omega t\right)$$

Thus, for positive *n*, the particles oscillate about the midplane with an amplitude of $z_{\max}$ and frequency of:

$$\omega_z = \sqrt{n}\omega$$

where ω is the orbit revolution frequency (the RF frequency). We then define ν_z:

$$\nu_z = \frac{\omega_z}{\omega} = \sqrt{n}$$

ν_z, the number of "betatron" oscillations per revolution, is called the "tune."

$\frac{d^2z}{d^2t} + n\omega^2 z = 0$ does not place an upper limit on *n* and the more positive *n* is, the greater the "restoring force" $\omega^2 nz$ will become.

Radial Stability: First let us consider the particle's angular acceleration A_r in polar coordinates:

$$A_r = \frac{d^2r}{dt^2} - r\left(\frac{d\theta}{dt}\right)^2 = \frac{d^2r}{dt^2} - \frac{v_\theta^2}{r}$$

Use A_r to describe equilibrium force established by the guiding field:

$$F_{eq} = MA_r = -qv_\theta B_z$$

(where we restrict the motion to the median plane). Re-arrange the above:

$$M\left(\frac{d^2r}{dt^2} - \frac{v_\theta^2}{r}\right) + qv_\theta B = 0$$

Of course the solution where *r* = constant, where $\frac{d^2r}{dt^2} = 0$, again reaches the equation of an ideal orbit:

$$\frac{mv_\theta^2}{r} = qv_\theta B$$

Now we ask if this is a stable orbit ? Let

$$r = r_e + x \quad \text{where} \quad x << r_e$$

where r_e is the equilibrium orbit, and *x* is a small excursion from that orbit. We write:

$$m\frac{d^2}{dt^2}\left(r_e + x\right) - \frac{mv^2}{r_e + x} + qvB_x = 0$$

where $B_x = B\left(r = r_e + x\right)$

and since $x << r_e$ we can write

$$\frac{1}{r_e + x} \approx \frac{1}{r_e}\left(1 - \frac{x}{r_e}\right).$$

Since r_e is constant,

$$m\frac{d^2}{dt^2}\left(x\right) - \frac{1}{r_e}\left(1 - \frac{x}{r_e}\right)mv^2 + qvB_x = 0$$

Substituting for r_e with:

$$r_e = \frac{mv^2}{qvB_e}$$

and after a little algebra we write:

$$m\frac{d^2x}{dt^2} + qv\left(B_x - B_e\right) + qvB_e\frac{x}{r_e} = 0$$

Since we are only considering small displacements, we can use the Taylor expansion:

$$B_x = B_e + x\frac{dB}{dr}$$

re-written as:

$$B_x - B_e = x\frac{dB}{dr}$$

Use $v \approx \omega r_e$,and divide through by *m* we get:

$$\frac{d^2x}{dt^2} + \frac{r_e}{B_e}\frac{dB}{dr}\omega^2 x = 0$$

Which of course can be re-written as:

$$\frac{d^2x}{dt^2} - n\omega^2 x + \omega^2 x = 0$$

Thus, again we arrive at the Kerst-Serber equation:

$$\frac{d^2x}{dt^2} + \omega^2(1-n)x = 0$$

Of course, the ideal radial orbit solution exists when $x = 0$, however an alternate solution yielding oscillatory motion occurs when *n* is less than 1.

$$x = x_{\max}\sin\left(\sqrt{1-n}\,\omega t\right)$$

Thus the frequency of motion is:

$$\omega_x = \omega\sqrt{1-n}$$

So the radial betatron "tune" is:

$$\nu_x = \frac{\omega_x}{\omega} = \sqrt{1-n}$$

Interestingly, in the radial focusing case, there is no lower limit on the value of *n*, it is only required that *n* remain below a value of 1 for radial stability, the smaller the *n* value, the greater the radial restoring force.

Complete transverse stability. It has thus been shown for axial stability, *n* must be greater than 0, and for radial stability *n* must be less than 1. Total transverse stability exists in the region of:

$$0 < n < 1$$

For details beyond the scope of this document, coupled resonances between the transverse motions further limit the value of *n*. *n* values of 0.2, 0.25, 0.33, 0.5 (and others higher) need to be avoided. Since, the ions to be accelerated begin at $r = 0$, $n = 0$ and will only climb as the radius increases. If $n = 0.2$ needs to be avoided, then the rate at which B_z decreases must be moderated such that only near the maximum ion radius does *n* approach 0.2. (for further details, the interested reader is referred to Livingood[3])

The following measurements and modeling indeed confirm, at least in the assumption of azimuthal symmetry, that our 12-inch magnet's field index runs from 0 to about 0.2 throughout the useful region for ion acceleration.

III. MEASUREMENTS. Drawing on the work of McClain and Friedman we briefly review the technique of the "1D" radial B_z-field measurement and present a typical data set.

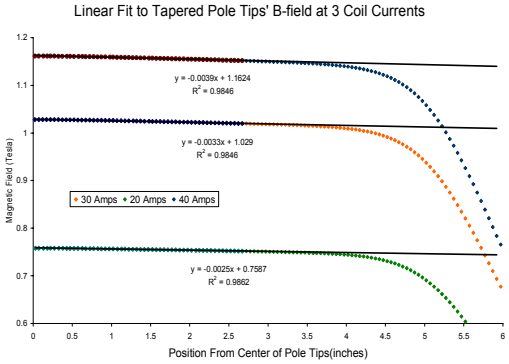

Fig.1 Radial measurements at three different magnet currents: 20, 30, & 40A

The profiling of the radial dependence of the magnetic field between the pole pieces required an experimental setup that allowed for acquisition of the magnetic field strength at precisely known positions with respect to the center of the pole pieces. In order to achieve this difficult goal, a Hall probe was mounted on a platform that was threaded onto a long screw (~12 in.) whose motion was driven by a computer-controlled stepper motor. This entire unit was set upon three adjustable "leveling" screws protruding from an aluminum mounting fixture secured to the bottom pole of the magnet. An aluminum fixture was used as not to distort the field and likewise the measurement. The three leveling screws allowed adjustment to ensure the probe's travel in the median plane. The Hall probe was connected to a Gauss meter whose analog recorder output was the input for a multimeter. The output of the multimeter was fed into a data acquisition unit, and the number of steps taken by the motor was read by the computers serial port. A LabView program wrote the gaussmeter's value and probe's position into a text file. The gauss meter was calibrated against a very well known NMR magnet, and a precisely located "magnetic needle" gave the probe's position calibration. For further details of the measurement the reader is refered to the work of McClain and Freidman[4]. Figure 1 shows typical field profiles at different levels of

magnetic excitation. Nominal magnet operation is about 32 amperes. Magnet data was taken at 20, 30, and 40 amperes to understand the effects of saturation on the field index, *n*.

We normalized the measured field profile for the three different operating currents: 20, 30, and 40 Amperes. Each field profile, as one would expect, had a peak field at $r = 0$. The data was linearly scaled to bring this peak field to unity. The simultaneous plotting of these normalized profiles, as shown in Figure 2, confirms that the field index's (*n*'s) profile does not vary with field strength, even into the beginning of the saturated régime. This generously allows for just one analysis of the field profile.

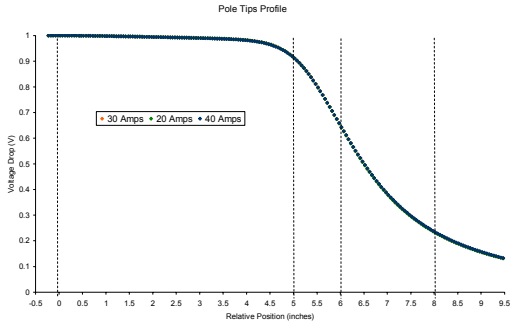

Fig.2 Simultaneous normalized field plot of the three current values: 20, 30, and 40 Amperes. The vertical dashed lines indicate, $r = 0$ – the center, $r = 5$ – the maximum ion radius, $r = 6$ – the pole tip edge, and $r = 8$ – the reference point.

IV. MODELING. Normally, computer based modeling of a complex device comes before the construction of the device. This was not the case with the 12-Inch cyclotron. Only recently has modeling software become available for our use. Los Alamos National Lab freely offers a 2D finite element modeling code named POISSON/SUPERFISH (PSF from now on).[5] This code can be applied to many problems, including electrostatics, RF cavities, and as utilized here, magnetostatics.

The first step in the modeling process was to import the 12-inch magnet's geometry into the PSF's input file. Because of the round pole tips, it seemed natural to take the 2D slice of the magnet in the plane where the pole tips were the widest – at one half of the depth of the magnet. Again, the 2D approximation is only valid when the magnet is considered in the non-saturated regime. With a nominal operating field of 1 Tesla this approximation becomes suspect. It should be noted that the pole tip material is fully annealed, hot rolled 1006 steel, possessing a very large μ.

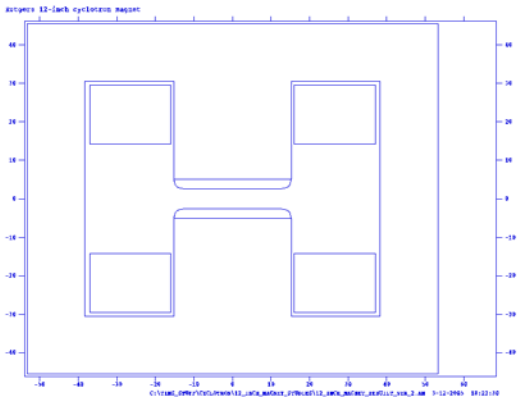

Fig.3 Magnet's input geometry

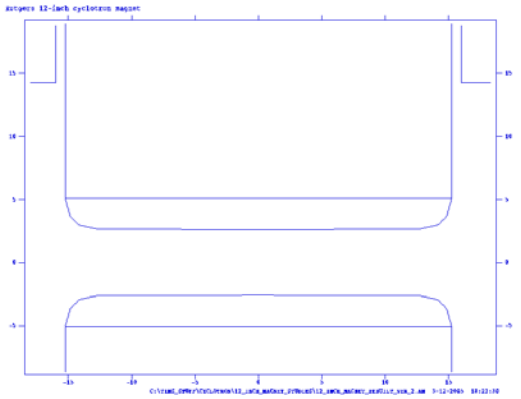

Fig.4 Close up shows slight gap increase.

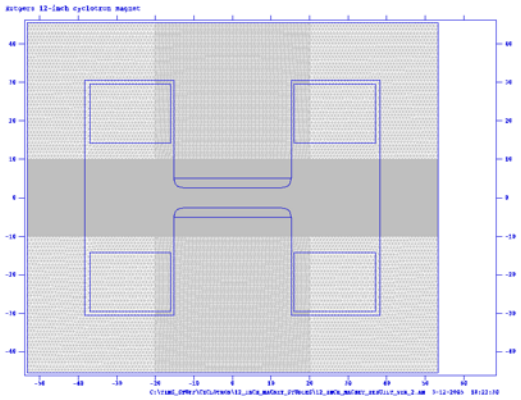

Fig.5 Varied mesh density displayed.

After the geometry was entered, PSF's solving mesh had to be described. To save computing time, a varied mesh was selected. The mesh was

made to be denser (thus higher resolution) in the region of interest, namely, between the poles, while setting a less dense mesh for regions of little interest. A greater number of horizontal mesh lines, as compared with vertical mesh lines, were required to resolve the slight inclination of the pole tips.

The coil current density was empirically set. The construction of the actual 12-inch cyclotron coils is unknown, as the coils came from a surplus source. The current density was varied in PSF through several points, until the peak 1.22 Tesla was achieved in the center of the gap. This corresponded to a PSF setting of 30,000 Ampere-turns.

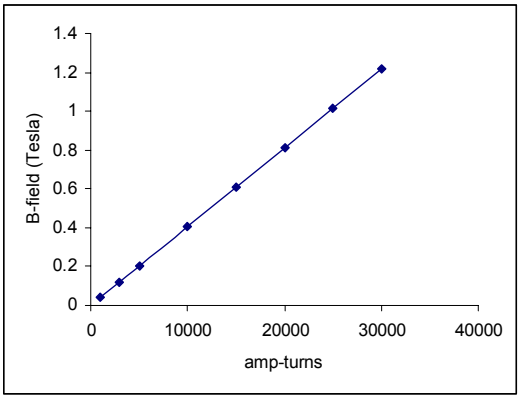

Fig.6 PSF B(i) curve, note lack of saturation

A comparison of PSF's output with the linear portion of the actual measured B(i) curve can yield insight into the construction of the coils, which was determined to be about 850 windings per coil.

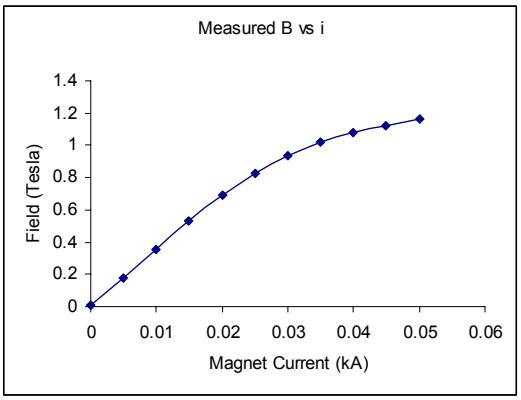

Fig.7 Actual measured B(i) curve

After solving PSF problem with a current density of 30,000Amp-Turns (the highest expected operating current density) the field vectors were plotted. This first successful display shows the field vectors hinting at the appropriate "bulging" of the magnet gap's field lines.

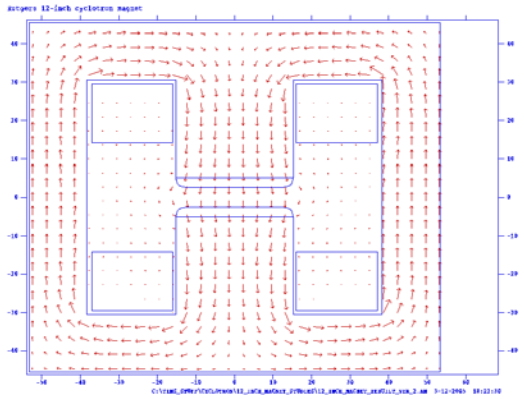

Fig.8 Plot of magnetic field vectors.

Certainly, the field contour lines provide a more instructive view of the field's behavior in the magnet circuit.

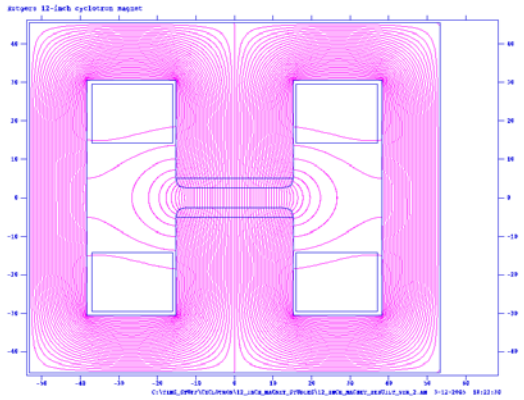

Fig.9 Plot of the magnetic field contours

Zooming in on the gap region, it is clear, though slight, that the gap linearly opens up with an increase of radius. Near the pole tip's edge, a rounded transition prevents localized saturation in the iron, thus radially extends the useful field region .

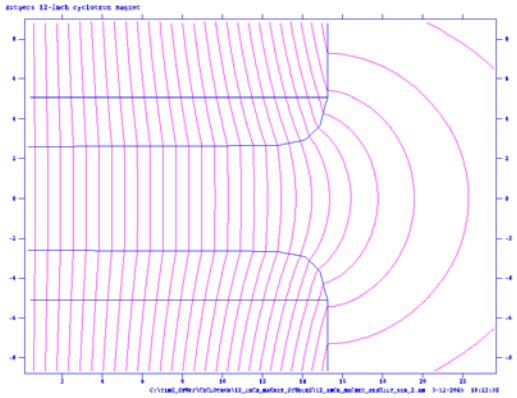

Fig.10 Close up of gap and contour lines.

The bulging can be more clearly seen in Figure 10. Using PSF's SF7 output generator, the field data was written to an Excel spread sheet, where the field index, *n*, was determined and plotted in Figure 11.

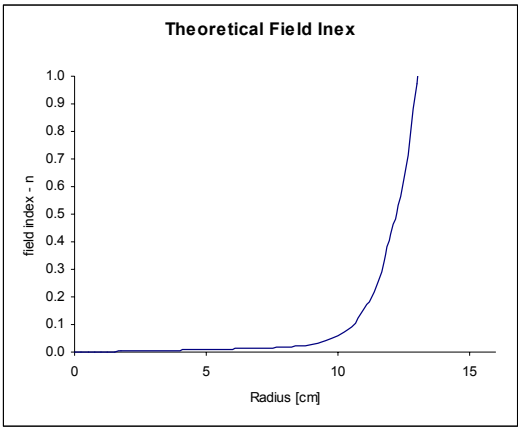

Fig.11 Modeled field index, *n*, as a function of radius.

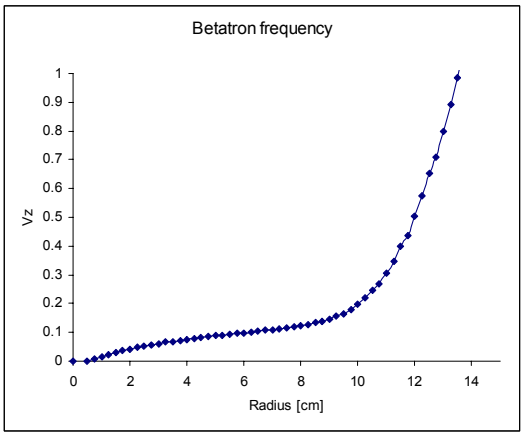

Fig.12 ν_z as a function of radius

The above analysis shows an ever increasing ν_z, with three clear regions of growth, see Figure 12. Initally, ν_z starts off at zero, climbs quickly up to a radius of 2 cm, then the increase takes on a slower rate of increase up to a radius of 9 cm. After 9 cm the rate if ν_z increase is exponential. Keep in mind that the maximum ion radius is 12.7 cm where ν_z reaches a value of 0.7 – well beyond the difference instability located at ν_z = 0.2, which comes at a radius of about 10 cm.

V. COMPARISON. It was very interesting to make the comparison between McClain and Friedman's measurements and PSF's output.

The measured field and modeled field were both normalized by, again, linearly scaling the fields such that the peak vertical field (occurring at *r* = 0 in both cases) was set to 1.0.

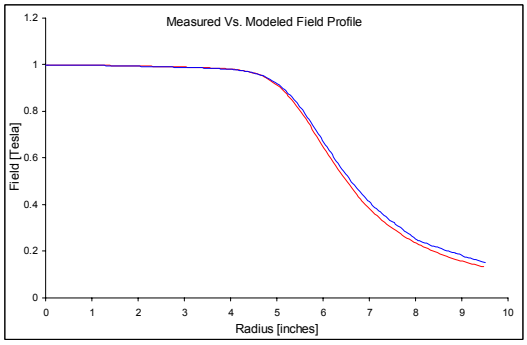

Fig.13 Measured and modeled radial field profiles

As shown in Figure 13 the profiles of the measured field and the modeled field are precisely matched in the region utilized for acceleration. This is an encouraging result, as pointed out earlier; the measured field profile followed a single line directly facing the magnet, while the modeled profile followed a single line 90° azimuthally from the measured path. If there was to be a discrepancy between the measured and modeled data, it would have been expected to be at a maximum difference between these two paths. A discrepancy does become pronounced at a radius greater than 6-inches, the "lower" strength field is the measured field. This is just as one would expect, as the measured path does does not have a vertical yoke piece to coral in the field lines, and thus they leak out easier.

The comparable profiles of the measured and modeled fields permits the acceptance of the modeled analyses of the field index *n* and the vertical betatron oscillations, ν_z.

VI. AVF FOCUSING STUDY. There is currently a program to obtain a 2D magnetic field map in an attempt to verify that our "1D" PSF approximation is indeed valid, and to further confirm our "1D" measured radial profile.

In the case that we do find an azimuthal field distortion, it will most likely have a periodicity of 2, which is inherently an unstable Azimuthal Varying Field (AVF) condition. A minimum periodicity of 3 is required for a stable operating point.

If in fact we find an AVF with a periodicity of 2, there are at least two possible paths to take. The first option is to "shim" out the AVF. By use of the 2-D field mapper, we can identify lulls in the field and manually install thin iron shims to shorten the gap and bring up the field to the desired value.

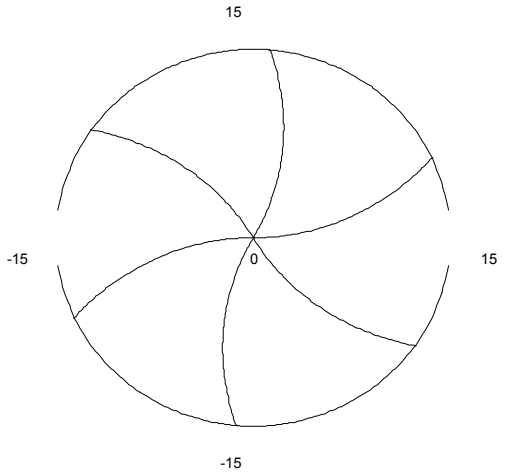

Fig.14 Top view of AVF pole tip with a slight Achimedian spiral edge.

The second option, posing more work, but which would provide a very interesting study, would be to introduce the use of an intentional strong AVF with a periodicity of at least 3. This academic exercise may provide the education needed to proceed in building an entire new chamber which supports an extracted beam. A detailed study has been completed by the author on the possibility of introducing AVF pole tips. We already posses the needed pole tip 1006 material and the required machine shop support.

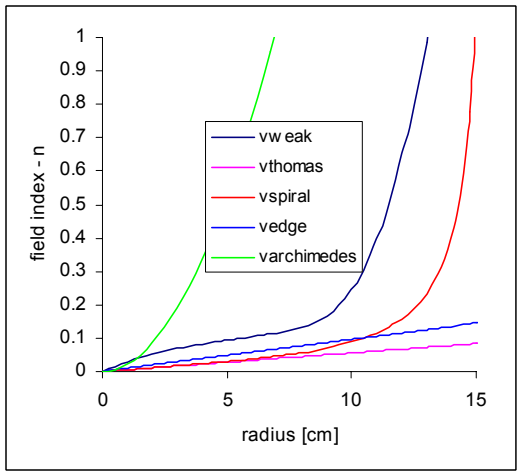

Fig.15 ν_z of different focusing methods

The light green trace (left and uppermost trace) in Figure 15 corresponds to the pole tip design shown in Figure 14. It is clear that ν_z grows very rapidly with even a slight spiral. Because of the cataclysmic beam instability at ν_z = 1, and other serious instabilities at ν_z = 0.2, 0.5 and so on, use of a spiral edge does not does not seem favorable.

The pink trace (lowest) in Figure 15 displays the sole effect of Thomas focusing, - AVF focusing without a spiral edge. It is interesting to note that in our case, weak focusing is in fact stronger than the colloquially termed AVF "strong focusing." This peculiararity arises from the fact that our small (1.2MeV) cyclotron does not noticeably suffer from relativistic effects. If it did, the magnetic field would need to increase with radius, as opposed to our decreasing field, in order to keep the more "massive" ions in step with the RF. As shown above, a defocusing effect would occur in the case of a larger cyclotron, where the vertical field needs to increase with radius (an increasing field forces *n* to be negative, thus axially unstable, or defocusing) – the effects of the increasing field can be offset with the use of Thomas focusing, and even further supplemented by use of spiral edges.

In the case that the 2D measurement actually yields a nice azimuthal symmetry, we will turn our investigation towards the ion source, as well as looking into the focusing effects of the "DEE-Dummy DEE" accelerating gap. Although shown that the "weak focusing" pole tips of our

small cyclotron should outperform AVF pole tips, it might still prove to be a useful exercise to procede with by another set of interested students.

VII. ACKNOWLEDGEMENTS. The author would like to thank the hard work of Stuart Hanebuth, William Schneider, and Dan Hoffman for building the precision measuring apparatus. The dedication and tenacity of the "cyclotron students," Chun, Mac Lynne, McClain, and Friedman needs to be applauded. Finally, many thanks to Prof Mohan Kalelkar for finding the required financial support, and for Prof's Gershenson and Thomson for lending the talent of their best students each year.

VIII. REFERENCES:

[1] Toni Feder "Building a Cyclotron on a Shoe string." *Physics Today*, November 2004, pages 30 - 31

[2]http://www.physics.rutgers.edu/cyclotron/papers/The_Cyclotron_Magnet_and_RF_Oscillator-low-quality.pdf

[3]J.J. Livingood, "Principles of Cyclic Particle Accelerators" D. Van Nostrand, 1961

[4]http://www.physics.rutgers.edu/cyclotron/papers/Profiling_the_Magnetic_Field_of_the_New_Pole_Tips.pdf

[5]http://laacg.lanl.gov/laacg/services/serv_access.phtml